Materials Chemistry and Physics 177 (2016) 164–170

Contents lists available at ScienceDirect

Materials Chemistry and Physics

journal homepage: www.elsevier.com/locate/matchemphys

Structural characterization of Fe–Pd nanowires grown by electrodeposition using an acid electrolyte

P. Domenichini [a], A.M. Condó [a, b], N. Haberkorn [a, b, *]

[a] Instituto Balseiro, Universidad Nacional de Cuyo, Av. Bustillo 9500, 8400 San Carlos de Bariloche, Argentina
[b] Centro Atómico Bariloche, Comisión Nacional de Energía Atómica, Av. Bustillo 9500, 8400 San Carlos de Bariloche, Argentina

HIGHLIGHTS

- Synthesis of Fe–Pd nanowires by electrodeposition is reported.
- Structural characterization of the nanowires by transmission electron microscopy.
- The synthesis of nanowires with austenitic phase is limited by fragile grain boundaries.

ARTICLE INFO

Article history:
Received 17 October 2015
Received in revised form
7 March 2016
Accepted 1 April 2016
Available online 7 April 2016

Keywords:
Alloys
Nanostructures
Chemical synthesis
Electron microscopy

ABSTRACT

$Fe_{70}Pd_{30}$ nanostructures have potential application in actuators due to their conventional and magnetic shape memory. Here, we report the microstructure of electrodeposition grown Fe–Pd nanowires in which the process was confined to polycarbonate membranes with a nominal pore diameter of 200 nm. We used an acid electrolyte (pH ≈ 5) in which the solution was stabilized with sulfosalicylic acid. The average chemical concentration of the nanowires can be systematically shifted from rich palladium to rich iron by changing the growth potential. The study of the microstructure by transmission electron microscopy indicates high chemical inhomogeneities due to phase coexistence between rich palladium regions (with FCC structure) and rich iron regions. The latter present a combination of BCC and amorphous phases. The average chemical composition of the nanowires can be better adjusted by using *a low frequency square* wave *voltage excitation* (alternating rich Pd and rich Fe regions). However, independently of the growth process, the nanowires morphology collapses after thermal annealing. This could be ascribed to fragile grain boundaries due to the presence of amorphous hydroxides and chemical impurities produced during the electrochemical process.

1. Introduction

The design of metallic nanostructures has potential applications in different nanotechnology fields [1,2]. Some of these applications include magnetic materials (for memory storage) [3] and microactuators based on shape memory alloys (SMAs) [4–6]. Furthermore palladium rich Fe–Pd alloys are interesting due to their catalytic activity and ability of palladium to absorb hydrogen [7]. Within SMAs two special types can be distinguished: alloys which present the shape memory effect (SME) and alloys which present the magnetic shape memory effect (MSM). SME appears in some metallic alloys and is associated with materials that can "recall" their low temperature shape after being heated and subsequently cooled. This phenomenon is associated with a martensitic transformation, which is a structural transformation without diffusion between a high temperature phase (called austenite) and a low temperature one (called martensite). The SME effect is a direct consequence of a reversible transformation between austenite and martensite. The MSM effect is present in some ferromagnetic alloys which exhibit significant changes in shape and size under applied magnetic field [8,9]. The mechanism is based on the magnetic-field-induced rearrangement of the crystallographic domains (martensite twin variants) produced by changes in the magnetization energy. The large strain provided by this mechanism is similar to the one obtained by a stress-induced one.

The MSM effect is present in numerous materials such as Ni–Mn–Ga [8] and Fe–Pd [9,10], among others. The Fe–Pd alloy

* Corresponding author. Centro Atómico Bariloche, Comisión Nacional de Energía Atómica, Av. Bustillo 9500, 8400 San Carlos de Bariloche, Argentina.
E-mail address: nhaberk@cab.cnea.gov.ar (N. Haberkorn).

http://dx.doi.org/10.1016/j.matchemphys.2016.04.013
0254-0584/

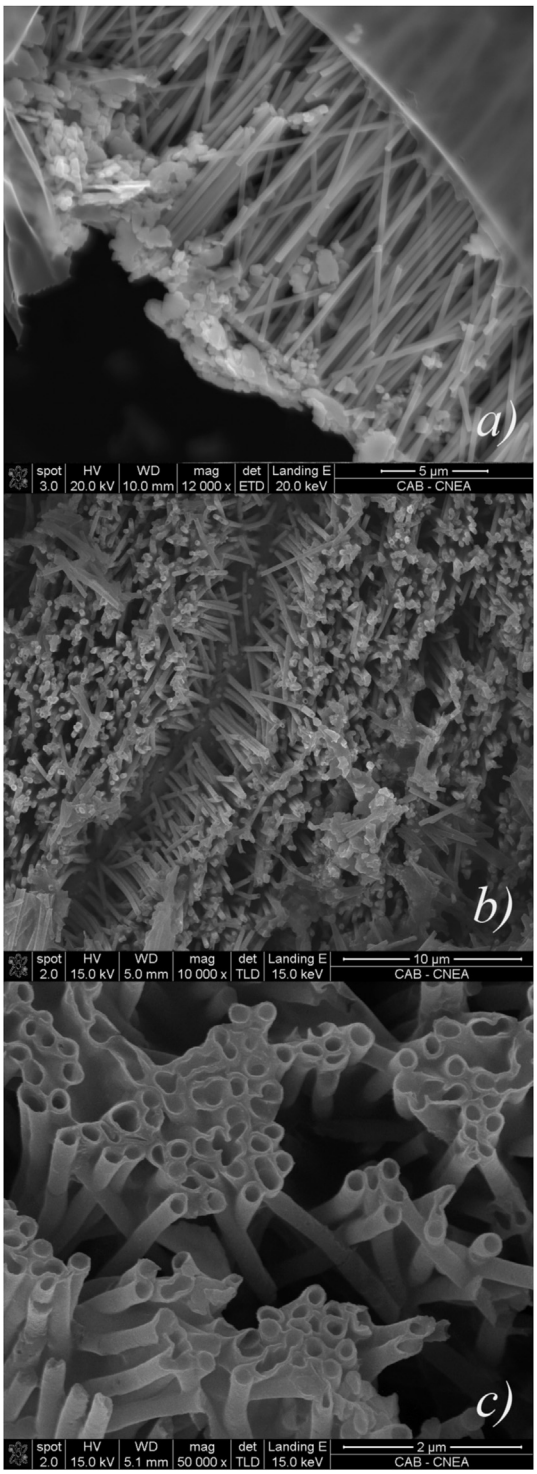

Fig. 1. SEM images of typical electrodeposited Fe–Pd nanowires obtained from the different growth voltages. *a)* Cross section image of nanowires embedded in the polycarbonate template. *b)* Plan-view image of nanowires embedded in the polycarbonate template. *c)* Image of the typical tubular structure observed in the nanowires.

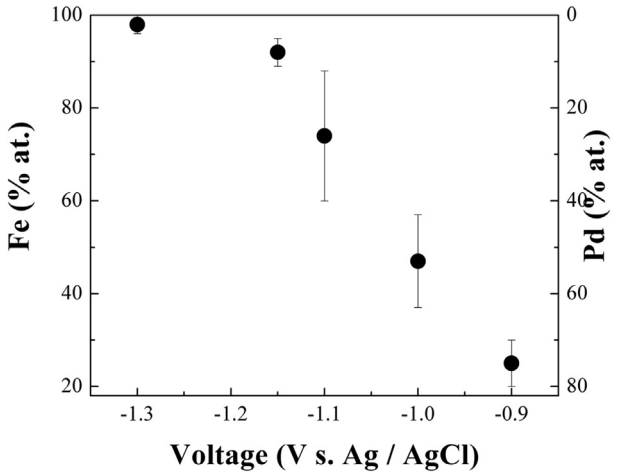

Fig. 2. Composition of Fe–Pd nanowires in polycarbonate membranes as function of deposition potential.

presents a small window of chemical concentration ($\approx Fe_{70}Pd_{30}$) for the MSM effect [7]. MSM nanostructures are usually based on sputtered thin films [11,12], nanopilars [13] and nanoparticles [14]. However, thin films [15] and nanowires (NWs) [16,17] of Fe–Pd grown by electrodeposition with potential MSM have been reported. As SMA properties are highly sensitive to small changes in the chemical composition, its fabrication by electrodeposition becomes hindered. For some alloys, the co-deposition is limited by the stability of the chemical solutions and by the reduction potential of the individual metals [18]. Two metals can be co-deposited if their respective potential E is (nearly) the same. Otherwise, codeposition can be obtained by adding a complexing agent which reduces the activity of the ions in the solution and displaces their redox potential. The Fe–Pd electrodeposition requires an appropriate complexing agent that would shift the reduction potential of palladium (Pd^0/Pd^{2+}: $E_0 = 0.95$ V) towards the less-noble iron (Fe^0/Fe^{2+}: $E_0 = -0.447$ V), while keeping the electrolyte chemically stable. Ammonia usually reduces the difference in E by the complex $Pd(NH_3)_4^{2+}$ [19]. Different electrolytes based on basic or acid bath stabilization have been used for the Fe–Pd system. The list includes baths based on the: ammonium tartrate [15,20], ammonium citrate [21,22] and sulfosalicylic acid [16,17,23], among others. The main difficulty in obtaining MSM in nanostructures grown by electrodeposition is ascribed to the presence of chemical inhomogeneities and nanometric grains. Both features act as barriers increasing the stress for twin boundary motion [24]. Chemical inhomogeneities are expected from phase coexistence between metastable and equilibrium phases [25,26], hydroxides [16] and chemical impurities of the electrochemical bath. The improvement of the chemical homogeneity and an appropriate microstructure can be achieved by thermal annealing [5,27].

The present paper examines the microstructure of Fe–Pd NWs (ø = 200 nm) grown by electrodeposition. We have used a sulfosalicylic acid based electrolyte (pH ≈ 5) [16,23]. The NWs were obtained by confining the electrodeposition process to a polycarbonate membrane with a nominal pore diameter (ø) of 200 nm. The NWs display solid and tubular geometries. The tubular geometry can be related with hydrogen evolution. The average chemical concentration of the NWs can be systematically shifted from rich Pd to rich Fe by changing the growth potential. The study of the microstructure indicates that the NWs show phase coexistence between rich palladium regions (with FCC structure) and rich iron regions. The latter present a combination of BCC and amorphous phases between grains. The average chemical composition of the NWs can be better adjusted by using a *low frequency square* wave *voltage excitation* (alternating segments with low over potential - Pd rich and with high over potential - Fe rich regions). However, independently of the growth process, the NWs are not stable

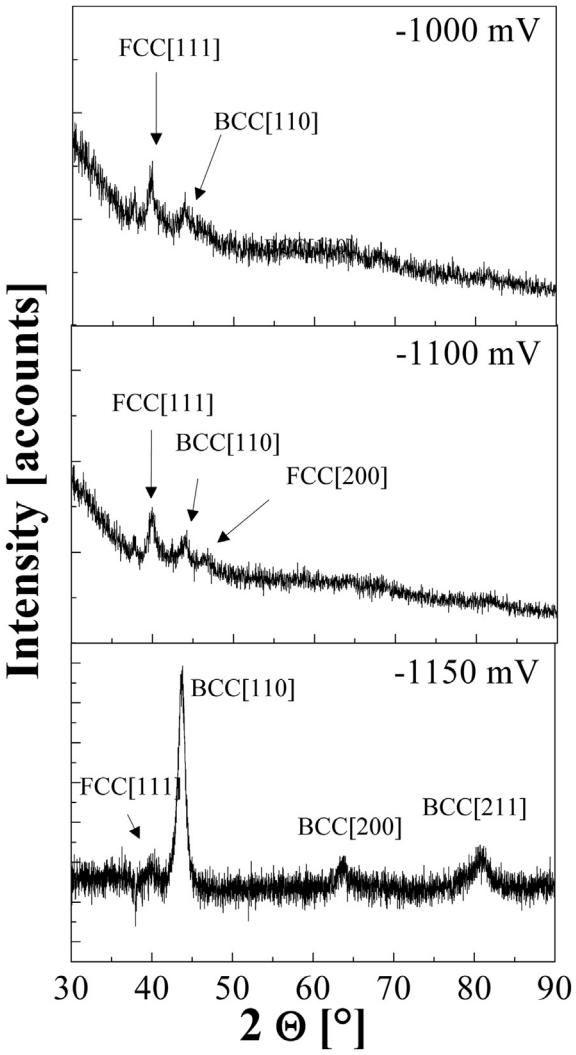

Fig. 3. X ray diffraction patterns of Fe–Pd nanowires grown at the voltages indicated in the panels.

during the thermal annealing (at temperatures suitable for the austenitic phase). Small fragments of NWs are often observed. This may be ascribed to fragile grain boundaries, caused by the presence of amorphous iron hydroxides which are produced during the electrochemical process.

2. Material and methods

The NWs were grown following the procedure described in Refs. [15,16]. The solution was prepared with commercially available chemicals (Aldrich). Water treated by a Millipore Milli-Q system was used. First, 1 g $PdCl_2$ was added to 2 ml concentrated hydrochloric acid. After complete dissolution, the solution became brown and transparent. A pink floc $Pd(NH_3)_2Cl_2$ appeared when the solution was dropped into 70 ml concentrated ammonia. The mixture was slowly heated and stirred until the floc disappeared and the solution turned clear [23]. Secondly, a solution of $FeSO_4{\cdot}7H_2O$ (0.1 M), sulfosalicylic acid $C_7H_6O_6S{\cdot}2H_2O$ (0.2 M) and $(NH_4)_2SO_4$ (0.3 M) was added to the first one (0.02 M). Finally, the bath was adjusted to pH ≈ 5 by H_2SO_4. The NWs were grown under stirring at room temperature. The working electrode was a commercial polycarbonate template (Millipore) with nominal pore size diameter of 200 nm with an area of ≈0.5 cm^2. A metallic Ag thin film was deposited by sputtering on one side of the porous membrane to serve as a cathode (the silver is connected with the solution across the pores). A commercial Ag/AgCl electrode was used as a reference, and a Pt wire as a counter. The NWs were grown at constant voltage (−0.9 V, −1.0 V, −1.15 V and −1.3 V vs. Ag/AgCl electrode). Wherever used, the deposition voltages refer to the Ag/AgCl electrode. The growth voltages were selected by considering ref. [16]. On the other hand, NWs were grown by using *a low frequency square* wave *voltage excitation* (SWVE) with −0.9 V (rich Pd) and −1.15 V (rich Fe) and the solution was purged beforehand by using pure nitrogen for 15 min. The electrode was submerged in the bath with the pore open side up so as to avoid hydrogen bubbles accumulation on the surface.

For the annealing, the polycarbonate template (with the Fe–Pd NWs embedded inside) was covered with tantalum foil, and encapsulated in a quartz ampoule (0.8 cm × 5 cm). The silver electrode was removed by using sandpaper. The ampoule was purged several times with Argon before being sealed. The sample was heated from room temperature to 1223 K at 5 K min^{-1} and was kept stable (at 1223 K) for approximately 120 min. Then, it was quenched in ice water. Annealing the NWs embedded in the polycarbonate template avoids the chemical reaction among themselves [5]. The annealing temperature was determined considering the stability for the austenitic phase [29].

The microstructure of the films was studied by transmission electron microscopy (TEM) with a Philips CM200UT microscope operating at 200 kV. Bundles of NWs embedded in the membrane were characterized by X-ray diffraction (XRD) in a Panalytical Empyrean equipment. Scanning electron microscopy (SEM) images were acquired with a FEI Nova NanoSEM 230. For the SEM images the polycarbonate membrane was partially dissolved in chloroform.

3. Results and discussion

Potentiostatic deposition experiments were carried out using the bath electrolyte previously described, at potentials between −0.9 V and −1.3 V vs. Ag/AgCl electrode. Fig. 1*a–b* show typical SEM images for the NWs partially embedded in the polycarbonate membrane. Most NWs look uniform and their lengths depend on the deposition time and the applied potential (being typically 1–3 μm/h). NWs with irregular sections appear as consequence of the pore diameter distribution. The NWs present solid and tubular geometries. The tubular geometry (see Fig. 1*c*) appears for all the voltages and can be related with hydrogen evolution and accumulation in the core of the pores (restrict the redox process to the pore wall). Although a higher hydrogen evolution is expected for NWs grown at more negative voltages, solid NWs are observed for rich Fe concentrations. This fact can be associated to the catalytic effect of Pd nanoclusters (present mainly at higher voltages) on hydrogen evolution [28]. The hydrogen bubbles might (partially or totally) block pores, reducing the deposition area and generating an inhomogeneous deposition morphology.

Fig. 2 shows the chemical composition of bundles of NWs as function of growth voltage by SEM EDS. Qualitatively, our results are similar to those reported in Ref. [16]. The chemical composition was obtained from the average of 5 measurements for all the voltages, except −1.1 V where the chemical composition was obtained from 10 measurements. Each measurement was performed in a different place of the template. The analyzed areas were 4 × 4 μm^2. The error bars correspond to the standard deviation. For low over potentials (−0.9 V) the NWs are rich in Pd. When the potential is reduced from −1.0 V to −1.1 V the Fe concentration increases from around 50 at % to 74 at %. It is important to mention

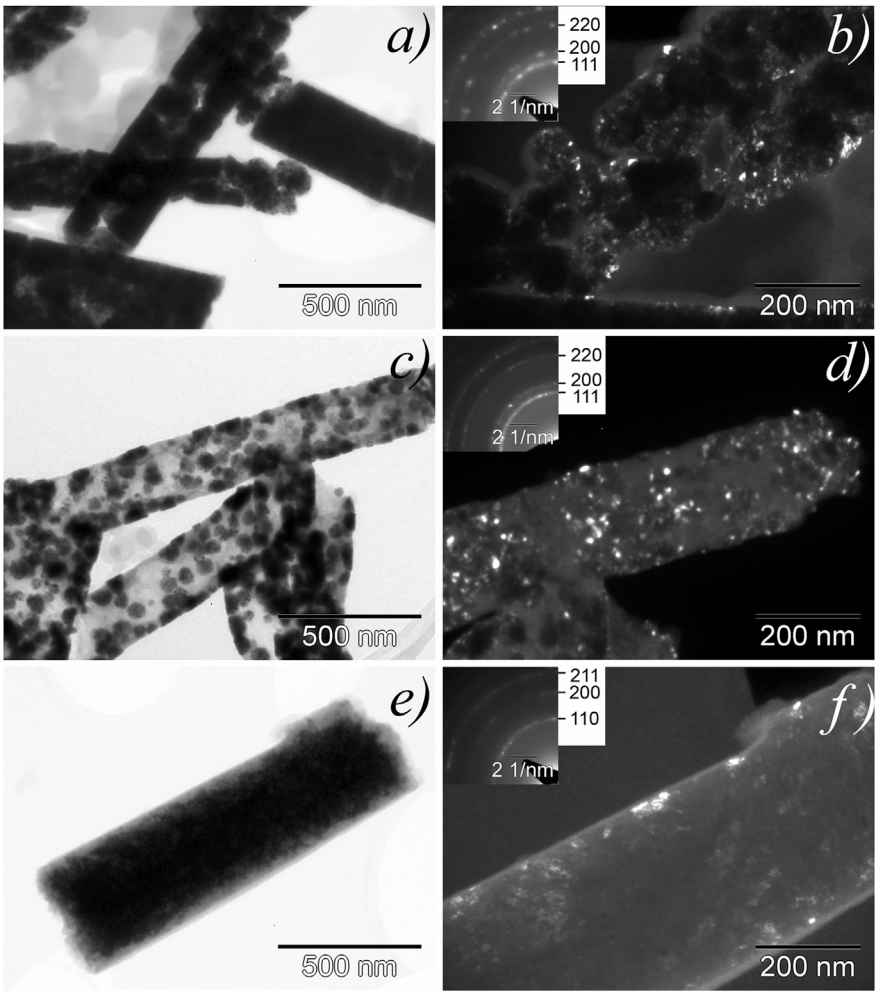

Fig. 4. Bright field (left column) and dark field (right column) TEM images of nanowires grown at the voltages: *a – b)* −0.9 V; *c – d)* −1.1 V; and *e–f)* −1.3 V. The insets correspond to the respective electron diffraction patterns.

that $Fe_{70}Pd_{30}$ corresponds to the desirable stoichiometry for martensitic transformation [9]. However, the large error bar obtained by EDS for −1.1 V indicates spatial chemical inhomogeneities on the template. Finally, at high over potentials (−1.15 V and −1.3 V), NWs rich in Fe are obtained.

XRD was performed to analyze the structure of the as-deposited NWs. Fig. 3 shows the results for the different growth voltages. At −1.0 V and −1.1 V, the NWs reveal phase coexistence among FCC (rich Pd) and BCC (rich Fe) structures. For the latter voltage, the error bar includes the $Fe_{70}Pd_{30}$ composition. Its size results as a consequence of high inhomogeneity (related to phase coexistence) and no codeposition among Fe and Pd at the desired chemical composition. Finally, at voltages lower than −1.15 V the XRD indicates mainly the presence of BCC structure.

The microstructure of the NWs was analyzed by TEM images. Fig. 4*a–f* show a summary of the results obtained for the different deposition potentials. Fig. 4*a–b* shows TEM images of granular microstructure in NWs grown at −0.9 V. According to the electron diffraction pattern (see Fig. 4*b* inset) and TEM-EDS analysis, the granular structures are rich in Pd (80 at % Pd – 20 at. % Fe) and they present the expected FCC structure. The grains are formed by many Pd nanoclusters with a typical size ≈7 nm (see dark field in Fig. 4*b*). Fig. 4*c–d* shows the TEM images for NWs grown at −1.1 V, which also present a granular structure. TEM-EDS analysis indicates that the grains are rich in Pd and the regions between the grains are rich in Fe (see Fig. 5*a–b*). In addition, the electron diffraction patterns reveal that the Pd rich regions are FCC (see Fig. 4*d* inset) and the matrix (between the Pd rich grains) presents an amorphous structure. The amorphous structure of the matrix can be associated with hydroxides generated by local changes in basic pH as consequence of hydrogen evolution (iron is unstable in basic pH solutions). It is important to mention that, although the BCC phase was not observed for −1.1 V by TEM, this phase was identified by XRD. The differences between TEM and XRD data can be attributed to the scale of the analyses. XRD provides information over bundles of NWs and TEM provides information on the most representative NWs of the batch. The presence of BCC phase (rich Fe) in the XRD data indicates that it should be present at least in a minor fraction of NWs for deposition voltages higher than −1.1 V Fig. 4e–*f* shows the TEM images for NWs grown at −1.3 V. Most NWs are rich in Fe and also reveal the expected BCC structure (see Fig. 4*f* inset). The analysis of the microstructure shows that, independently of the growth voltage, the NWs display a clear phase separation between rich Pd and rich Fe regions. Fig. 5*a–b* reveal, that for voltages higher than −1.1 V, Pd rich nanoparticles appear embedded in matrix composed mainly by Fe and O (possibly $Fe(OH)_2$). These results indicate that, by using the specified chemical bath, no codeposition at the desired chemical concentration occurs. The presence of large amorphous Fe phases and inhomogeneities for NWs with average chemical composition close to $Fe_{70}Pd_{30}$, hinders the possibility of

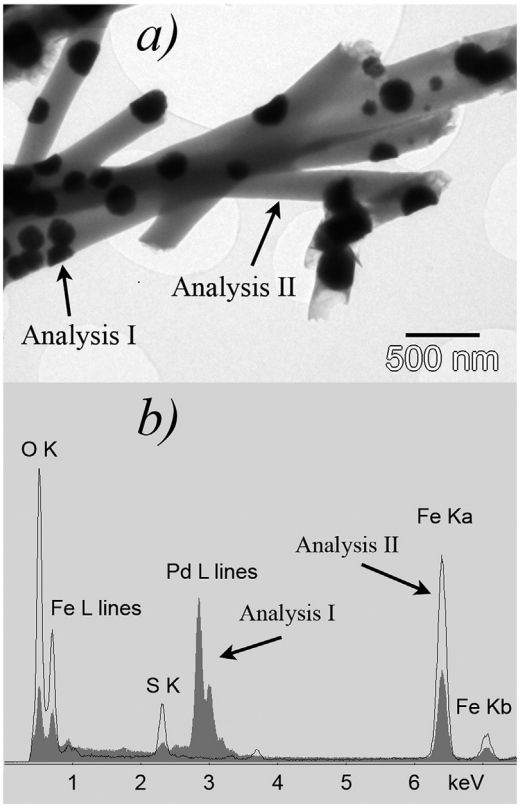

Fig. 5. *a)* Bright field TEM images of NWs grown at −1.0 V *b)* EDS analyses for the regions I and II indicated in *a)*.

sintering NWs with austenitic phase, using a single step deposition potential.

An alternating potential mode has been proposed to improve homogeneity and to adjust the chemical composition close to $Fe_{70}Pd_{30}$ [16,17]. Different baths of NWs were obtained by alternating −0.9 V and −1.15 V. The potentials correspond to rich Pd and rich Fe NWs in Fig. 2. The average chemical composition can be modified by changing the number of periods and the deposition time for each voltage. Fig. 6*a* shows the chemical composition of the NWs as function of the time ratio (−0.9 V/−1.15 V). The values were calculated from 10 independent measurements of EDS-SEM performed in different regions of the template. The analyzed areas were $4 \times 4\ \mu m^2$. It is noticeable that the standard deviation decreases for the desirable $Fe_{70}Pd_{30}$ in comparison with NWs grown by using a single step deposition potential [16]. In addition, most NWs present solid structures (see Fig. 6*b*), which is different from those obtained using a single voltage. Fig. 6*c* shows the typical modulated structures obtained in the NWs by using a SWVE with −0.9 V (100 seg)/−1.15 V (100 seg). The chemical composition for the modulated structure is indicated in Fig. 6*d*. Regions I are rich in Fe (−1.15 V) whereas region II displays higher chemical concentration of Pd. A striking feature of the modulated structures is the presence of BBC iron (see inset Fig. 6*c*) instead of the amorphous phase typically observed in Fig. 4*a* and *c*. This fact indicates that both, more accurate chemical composition and a reduction of amorphous phases can be obtained using SWVE. Although the results are not included, a minor fraction of inhomogeneous and non-modulated structures are also observed in the NWs bundles. The inhomogeneous distribution of microstructures can be attributed to hydrogen evolution, which might (partially or totally) block pores. Furthermore, as OH− ion is produced by water reduction,

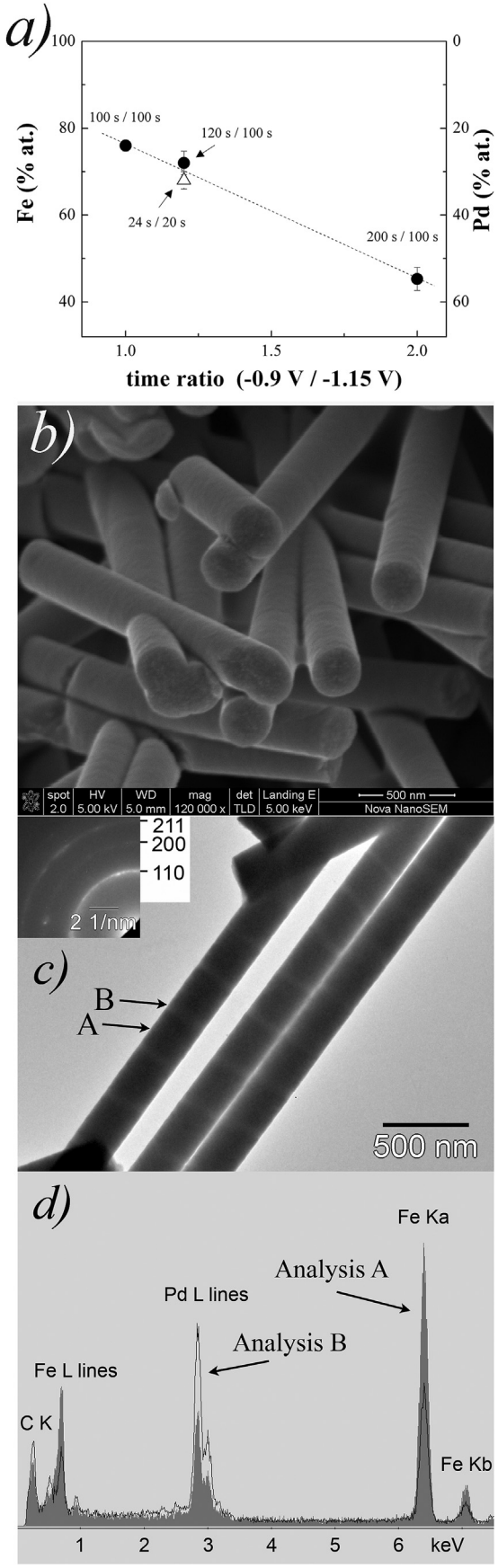

Fig. 6. *a)* Composition of Fe–Pd NWs grown using SWVE (− 0.9 V/−1.15 V) as function of the time ratio at the respective voltages. *b)* SEM image of typical electrodeposited Fe–Pd nanowires grown using SWVE. *c)* Bright field TEM for NWs grown using SWVE with time ratio 1. *Inset*: *corresponding electron diffraction pattern of the region A.* d) EDS analyses for the A–B regions indicated in *c*.

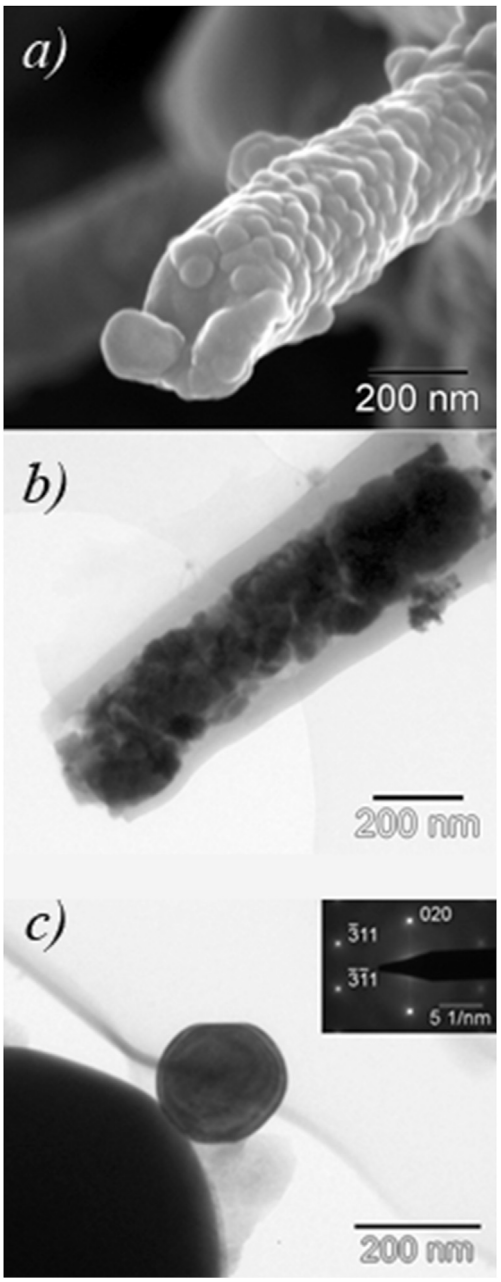

Fig. 7. *a)* SEM image of a typical annealed Fe–Pd nanowire. *b)* Bright field TEM image of a typical fragment of an annealed rich Fe nanowire after being dispersed in ethanol by ultrasound. *c)* Bright field TEM image of a typical nanoparticle observed (after annealing) in Fe–Pd NWs grown by using a *SWVE*. *Inset*: *corresponding electron diffraction pattern of the nanoparticle*.

local changes in pH within the pores are expected to modify the stability of the bath, facilitating the precipitation of hydroxides such as $Fe(OH)_2$.

Finally, different batches of Fe–Pd NWs grown by using constant potential and a SWVE were encapsulated and annealed at 1173 K for 2 h. The annealed temperature was selected considering the thermal equilibrium for the austenite phase [29]. Two different types of results (depending on the chemical composition) were observed. The NWs grown by using constant potential higher than −1.1 V usually collapse during the annealing. Rich Fe NWs, grown at more negative deposition voltages (−1.15 V to −1.3 V), present an extremely fragile granular structure (see Fig. 7*a*). Fig. 7*b* shows a typical TEM image of rich Fe fragments of NWs after being dispersed by ultrasound. This fragility is also observed in NWs grown by using SQVR. Frequently, rich Pd and Fe–Pd nanospheres and small fragments of NWs of different chemical composition ($Fe_{50}Pd_{50}$ and $Fe_{1-x}Pd_x$) are observed after annealing. Fig. 7*c* shows a typical nanosphere with chemical concentration ≈ $Fe_{65}Pd_{35}$. The inset in Fig. 7*c* corresponds to the electron diffraction pattern expected for the austenitic phase (FCC). However, as mentioned above, a high dispersion of morphologies and chemical concentration is observed in the residues of the annealed NWs. The high fragility of the NWs can also be associated with chemical segregation of hydroxides and chemical residues (i. e. sulfur) which weaken the grain boundaries.

The results indicate that several limitations exist in the synthesis of Fe–Pd NWs with austenitic phase by using an acid bath with Fe^{2+}/Pd^{2+} complexes. According to the present study, no codeposition at the desired chemical concentration occurs using a single step potential. High spatial chemical inhomogeneity in the arrays of NWs is observed to the $Fe_{70}Pd_{30}$ chemical composition. In addition, a clear phase separation between Pd-rich and Fe-rich regions was observed by TEM. Although a rich Fe BCC phase appears in the XRD for all the deposition voltages (see Fig. 3), TEM specimens show that at voltages higher than −1.1 V the Fe is mostly present as amorphous phases separating rich Pd grains. We have not observed coexistence of FCC (Pd) and BCC (Fe) phases by TEM in the nanoscale for NWs grown in a single step deposition for all the studied voltages. Usually, high hydrogen evolution (manifested as bubbles) is observed for all the used deposition potentials. The catalytic effect of Pd nanoclusters on the electrolysis of the water is evident because solid nanowires are mainly observed for chemical composition rich in Fe. The presence of amorphous iron phases can be associated with local changes in the pH within the pores originated by electrolysis of the water. In addition, although the use of SWVE allows the synthesis of solid NWs with adequate chemical composition (depending on the time ratio), the morphology collapses during the thermal annealing. This suggests that the presence of amorphous phases between grains weakens the NWs. The last observation is in agreement with the fragility observed in rich Fe NWs obtained by using a single step potential.

Finally, it is worth mentioning the possibility to extend the actual study to other chemical baths [17,30]. Substitution of Fe^{2+} by Fe^{3+} improves the homogeneity of NWs grown using pulse plating techniques [17]. On the other hand, basic baths [30] have been successively used in the synthesis of Fe–Pd NWs with chemical composition in the range of $Fe_{70}Pd_{30}$. However, non-detailed information about the microstructure has been provided. The presence of phase coexistence for NWs produced by a single step deposition or by using pulsed techniques requires thermal annealing at temperatures that stabilize the austenitic structure. Thus, the morphological stability of the annealed NW arrays is crucial in the design of martensitic nanostructures. Eliminating the precipitation of amorphous structures during the electrochemical process is essential to avoid fragile grain boundaries. Thermal annealing produces chemical homogenization [5], eliminates possible metastable phases [10,26] and increase the grain size [24].

4. Conclusions

Fe–Pd NWs were grown by electrodeposition, confining the process to a polycarbonate membrane with a nominal pore diameter of 200 nm. An electrolyte based on acid bath (pH ≈ 5) was used, which was based on the stabilization of the solution using sulfosalicylic acid. The NWs presented solid and tubular geometries. The tubular geometry can be related with hydrogen evolution. The average chemical concentration of the samples can be

systematically shifted from rich in palladium to rich in iron by changing the deposition potential. However, the nanowires revealed phase coexistence among rich Pd regions (with FCC structure) and rich Fe regions. The rich Fe regions indicated a combination of BCC and amorphous phases (hydroxides). No codeposition at the desired chemical concentration occurred under the acid electrolyte previously described. In addition, segmented nanowires (with rich Pd and rich Fe regions) were grown by using a SWVE. Although the average chemical composition of the NWs can be better adjusted to the desirable one for MSM ($Fe_{70}Pd_{30}$), the resulting NWs (after thermal annealing to desirable temperatures for austenitic phase (and alloying)) are extremely fragile. This fact can be attributed to chemical segregation towards grain boundaries. The presence of austenitic phase was only observed in nanoparticles produced by the thermal annealing (fragments of NWs).

Acknowledgements

We thank P. Troyon, M. Corte, E. Aburto, M. Isla, C. Gómez Bastidas and D. Wilberger for technical assistance. This work has been supported by Agencia Nacional de Promoción Científica y Tecnológica PICT 2012-0884. N. H is member of the Instituto de Nanociencia y Nanotecnología (Argentina). N. H. and A. M. C. are members of CONICET (Argentina).

References

[1] C.N.R. Rao, F.L. Deepak, G. Gundiah, A. Govindaraj, Inorganic nanowires, Prog. Solid State Chem. 31 (2003) 5–147.
[2] D.J. Sellmyer, M. Zheng, R. Skomski, Magnetism of Fe, Co and Ni nanowires in self-assembled arrays, J. Phys. Condens. Matter 13 (2001) R433–R460.
[3] T.M. Whitney, J.S. Jiang, P.C. Searson, C.L. Chien, Fabrication and magnetic properties of arrays of metallic nanowires, Science 261 (1993) 1316–1319.
[4] Francis R. Phillips, Dong Fang, Hongxing Zheng, Dimitris C. Lagoudas, Phase transformation in free-standing SMA nanowires, Acta Mater 59 (2011) 1871–1880.
[5] N. Haberkorn, A.M. Condó, M. Sirena, F. Soldera, F.C. Lovey, Single crystalline β phase Cu-Zn nanowires: synthesis and martensitic transformation, Mat. Lett. 124 (2014) 256–260.
[6] Anja Backen, Srinivasa R. Yeduru, Manfred Kohl, Stefan Baunack, Anett Diestel, Bernhard Holzapfel, Ludwig Schultz, Sebastian Fähler, Comparing properties of substrate-constrained and freestanding epitaxial Ni–Mn–Ga films, Acta Mater 58 (2010) 3415–3421.
[7] M.H. Martin, A. Lasia, Electrochim. Acta 53 (2008) 6317–6322.
[8] A. Sozinov, A.A. Likhachev, N. Lanska, K. Ullakko, Giant magnetic-field-induced strain in NiMnGa seven-layered martensitic phase, Appl. Phys. Lett. 80 (2002) 1746–1748.
[9] Tokujiro Yamamoto, Minoru Taya, Yuji Sutou, Yuanchang Liang, Taishi Wada, Larry Sorensen, Magnetic field-induced reversible variant rearrangement in Fe–Pd single crystals, Acta Mater 52 (2004) 5083–5091.
[10] J. Cui, T.W. Shield, R.D. James, Phase transformation and magnetic anisotropy of an iron–palladium ferromagnetic shape-memory alloy, Acta Mater 52 (2004) 35–47.
[11] V.A. Chernenko, M. Kohl, M. Ohtsuka, T. Takagi, V.A. L'vov, V.M. Kniazky, Thickness dependence of transformation characteristics of Ni–Mn–Ga thin films deposited on alumina: experiment and modeling, Mater. Sci. Eng. A 438–440 (2006) 944–947.
[12] T. Edler, S.G. Mayr, Film lift-off from MgO: freestanding single crystalline Fe-Pd films suitable for magnetic shape memory actuation - and beyond, Adv. Mater. 22 (2010) 4969–4972.
[13] N. Ozdemir, I. Karaman, N.A. Mara, Y.I. Chumlyakov, H.E. Karaca, Size effects in the superelastic response of $Ni_{54}Fe_{19}Ga_{27}$ shape memory alloy pillars with a two stage martensitic transformation, Acta Mater 60 (2012) 5670–5685.
[14] Kenta Seki, Hiroaki Kura, Tetsuya Sato, Tomoyasu Taniyama, Size dependence of martensite transformation temperature in ferromagnetic shape memory alloy FePd, J. Appl. Phys. 103 (2008) 063910–063919.
[15] Feng Wang, Sayaka Doi, Kaori Hosoiri, Hirohisa Yoshida, Toshio Kuzushima, Masao Sasadaira, Torhu Watanabe, Nanostructured Fe–Pd thin films for thermoelastic shape memory alloys—electrochemical preparation and characterization, Electrochim. Acta 51 (2006) 4250–4254.
[16] V. Haehnel, S. Fähler, L. Schultzb, H. Schlörb, Electrodeposition of $Fe_{70}Pd_{30}$ nanowires from a complexed ammonium–sulfosalicylic electrolyte with high stability, Electrochem. Commun. 12 (2010) 1116–1119.
[17] Veronika Haehnel, Christine Mickel, Sebastian Fähler, Ludwig Schultz, Heike Schlörb, Structure, microstructure, and magnetism of electrodeposited $Fe_{70}Pd_{30}$ nanowires, J. Phys. Chem. C 114 (2010) 19278–19283.
[18] Frederick A. Lowenheim, Modern Electroplating, third ed., John Wiley & Sons, New York, 1973.
[19] M.E. Baumgärtner, D.R. Gabe, Palladium-iron alloy electrodeposition. Part I. Single metal systems, Trans. IMF 78 (2000) 11–16.
[20] Sayaka Doi, Feng Wang, Kaori Hosoiri, Tohru Watanabe, Preparation and characterization of electrodeposited Fe–Pd binary alloy film, Mater. Trans. 44 (2003) 649–652.
[21] S.C. Hernández, B.Y. Yoo, E. Stefanescu, S. Khizroev, N.V. Myung, Electrodeposition of iron–palladium thin films, Electrochim. Acta 53 (2008) 5621–5627.
[22] Darja Pečko, Nina Kostevšek, Boris Pihlar, Zoran Samardžija, Spomenka Kobe, Kristina Žužek Rožman, Electrochemical studies of Fe and Pd deposition and their influence on the co-deposition of the Fe–Pd alloy, J. Electroanal. Chem. 738 (2015) 51–60.
[23] X. Fei, S. Tang, R. Wang, H. Su, Y. Du, Fabrication and magnetic properties of Fe–Pd nanowire arrays, Solid State Commun. 141 (2007) 25–28.
[24] T. Waitz, V. Kazykhanov, H.P. Karnthaler, Martensitic phase transformations in nanocrystalline NiTi studied by TEM, Acta Mater. 52 (2004) 137–147.
[25] P.L. Cavallotti, L. Nobili, A. Vicenzo, Phase structure of electrodeposited alloys, Electrochim. Acta 50 (2005) 4557–4565.
[26] Sergey V. Barabash, Roman V. Chepulskii, Volker Blum, Alex Zunger, First-principles determination of low-temperature order and ground states of Fe-Ni, Fe-Pd, and Fe-Pt, Phys, Rev. B 80 (2009) 220201(1)–220201(4).
[27] C. Espinoza Torres, A.M. Condó, N. Haberkorn, E. Zelaya, D. Schryvers, J. Guimpel, F.C. Lovey, Structures in textured Cu–Al–Ni shape memory thin films grown by sputtering, Mater. Charact. 96 (2014) 256–262.
[28] L.A. Kibler, Dependence of electrocatalytic activity on film thickness for the hydrogen evolution reaction of Pd overlayers on Au(1 1 1), Electrochim. Acta 53 (2008) 6824–6828.
[29] P. Franke, D. Neuschütz, SGTE, Landolt-Börnstein-Group IV Physical Chemistry, Binary Systems. Part 3: Binary Systems from Cs-K to Mg-Zr, Springer, Berlin Heidelberg, 2005.
[30] Nina Kostevšek, Kristina Žužek Rožman, Darja Pečko, Boris Pihlar, Spomenka Kobea, A comparative study of the electrochemical deposition kinetics of iron-palladium alloys on a flat electrode and in a porous alumina template. Electrochim, Acta 125 (2014) 320–329.